

## Article

# Mechanical Properties and Creep Behavior of Undoped and Mg-Doped GaN Thin Films Grown by Metal–Organic Chemical Vapor Deposition

Ali Khalfallah<sup>1,2,3,\*</sup>  and Zohra Benzarti<sup>1,4,5</sup> 

<sup>1</sup> CEMMPRE, Department of Mechanical Engineering, University of Coimbra, Rua Luís Reis Santos, 3030-788 Coimbra, Portugal; zohra.benzarti@ua.pt

<sup>2</sup> Laboratoire de Genie Mécanique, Ecole Nationale d'Ingénieurs de Monastir, Université de Monastir, Av. Ibn El-Jazzar, Monastir 5019, Tunisia

<sup>3</sup> DGM, Institut Supérieur des Sciences Appliquées et de Technologie de Sousse, Université de Sousse, Cité Ibn Khaldoun, Sousse 4003, Tunisia

<sup>4</sup> Laboratory of Multifunctional Materials and Applications (LaMMA), Department of Physics, Faculty of Sciences of Sfax, University of Sfax, Soukra Road km 3.5, B.P. 1171, Sfax 3000, Tunisia

<sup>5</sup> Department of Electronics, Telecommunications and Informatics (DETI), University of Aveiro, Campus Universitário de Santiago, 3810-193 Aveiro, Portugal

\* Correspondence: ali.khalfallah@dem.uc.pt; Tel.: +351-931-491-650

**Abstract:** This paper investigates the mechanical properties and creep behavior of undoped and Mg-doped GaN thin films grown on sapphire substrates using metal–organic chemical vapor deposition (MOCVD) with trimethylgallium (TMG) and bis(cyclopentadienyl)magnesium (Cp<sub>2</sub>Mg) as the precursors for Ga and Mg, respectively. The Mg-doped GaN layer, with a [Mg]/[TMG] ratio of 0.33, was systematically analyzed to compare its mechanical properties and creep behavior to those of the undoped GaN thin film, marking the first investigation into the creep behavior of both GaN and Mg-doped GaN thin films. The results show that the incorporated [Mg]/[TMG] ratio was sufficient for the transition from n-type to p-type conductivity with higher hole concentration around  $4.6 \times 10^{17} \text{ cm}^{-3}$ . Additionally, it was observed that Mg doping impacted the hardness and Young's modulus, leading to an approximately 20% increase in these mechanical properties. The creep exponent is also affected due to the introduction of Mg atoms. This, in turn, contributes to an increase in pre-existing dislocation density from  $2 \times 10^8 \text{ cm}^{-2}$  for undoped GaN to  $5 \times 10^9 \text{ cm}^{-2}$  for the Mg-doped GaN layer. The assessment of the creep behavior of GaN and Mg-doped GaN thin films reveals an inherent creep mechanism governed by dislocation glides and climbs, highlighting the significance of Mg doping concentration in GaN thin films and its potential impact on various technological applications.

**Keywords:** MOCVD; Mg-doped GaN layers; point defects; nanoindentation; creep behavior



**Citation:** Khalfallah, A.; Benzarti, Z. Mechanical Properties and Creep Behavior of Undoped and Mg-Doped GaN Thin Films Grown by Metal–Organic Chemical Vapor Deposition. *Coatings* **2023**, *13*, 1111. <https://doi.org/10.3390/coatings13061111>

Academic Editor: Andrey V. Osipov

Received: 18 May 2023

Revised: 12 June 2023

Accepted: 14 June 2023

Published: 16 June 2023



**Copyright:** © 2023 by the authors. Licensee MDPI, Basel, Switzerland. This article is an open access article distributed under the terms and conditions of the Creative Commons Attribution (CC BY) license (<https://creativecommons.org/licenses/by/4.0/>).

## 1. Introduction

Group III-nitrides, such as GaN, are wide-bandgap semiconductor materials (3.4 eV) that gained significant attention in optoelectronic devices due to their superior optical properties. The Mg-doped GaN is particularly important as it can enable reproducible p-type conductivity, which is essential for the development of high-efficiency light emitting diode LEDs and laser diodes [1–3]. Successful preparation of p-type Mg-doped GaN layers is one of the vital challenges for realizing blue, green LEDs, and high-power devices [4,5]. The electrical and optical characteristics of GaN and Mg-doped GaN were extensively explored to better understand their behavior and optimize their quality [6–8]. In addition to probing the latter features, the mechanical properties of GaN layers are also important for functional components in optoelectronic devices. Therefore, investigating the impact of Mg doping on the mechanical properties of GaN layers is crucial. Specifically, when GaN

layers are subjected to high gradients of temperature and electric and/or stress fields, their performance may deteriorate and they may experience changes in their electric, optical properties, and structural damage. These changes potentially lead to device failure. The analysis of the mechanical behavior of GaN and Mg-doped GaN layers contributes to optimizing film quality and realizing the full potential of these devices.

However, the available literature indicates that there is limited research addressing the determination of the mechanical properties of Young's modulus and hardness of GaN thin films [9], and more specifically, Mg-doped GaN thin films [10]. Furthermore, there is a paucity of literature on plasticity-dependent time tests such as creep nanoindentation for GaN thin films [11]. Despite the significance of investigating their creep behavior, which is critical for designing and optimizing sensors, actuators, and RF devices, there are limited studies on it. This lack impedes our understanding of the creep behavior and its impact on the long-term stability and reliability of power electronics, MEMS, and optoelectronics devices [12–14]. Therefore, the justification for conducting further investigation into the creep behavior of material thin films, especially for semiconductors, is evident.

This study attempts to fill this gap in the literature by investigating the creep behavior of undoped GaN and Mg-doped GaN thin films. The study demonstrates that Mg doping in GaN layers leads, on one hand, to a transition from n-type (GaN layer) to p-type conductivity (Mg-doped GaN layer), resulting in high hole concentration favorable for high blue luminescence, and on the other hand, to an increase in defects and the disappearance of pop-ins observed in nanoindentation curves of Mg-doped GaN layers. Indeed, the presence of controlled defects in GaN layers can be advantageous in achieving a balance between optimal physical properties and mechanical characteristics for the development of functional and high-strength semiconductor materials. These materials showed potential for use in optoelectronic devices, as was demonstrated for Al-doped GaN films [15]. In addition, it is shown that the creep behavior of the GaN layer was influenced by the introduction of defects, leading to a decrease in creep stress exponent and creep depth, which suggests a creep mechanism governed by dislocation glides and climbs. These findings can provide valuable insights into the design and optimization for a wide range of GaN-based technological applications.

## 2. Materials and Methods

Mg-doped GaN layers were grown on c-(0001) plane sapphire substrates using a vertical MOCVD reactor. TMG and ammonia (NH<sub>3</sub>) were used as the precursors for Ga and N, respectively, while Cp<sub>2</sub>Mg was used as the Mg source. The flow rate of Cp<sub>2</sub>Mg was set to 20 μmol/min, while the flow rate of TMG was maintained at 7 μmol/min, resulting in a [Mg]/[TMG] ratio of 0.33. Prior to the growth of GaN layers, a 30 nm-thick low-temperature buffer layer was grown at 600 °C for 10 min for both undoped and Mg-doped GaN layers to enhance the quality of the substrate–layer interface and thus to reduce the mismatch. Subsequently, the temperature was increased from 600 °C to 1100 °C to initiate the deposition of the undoped GaN or the Mg-doped GaN layers. Both samples were grown under a mixture of N<sub>2</sub> and H<sub>2</sub> carrier gas. The carrier gas flux of N<sub>2</sub> and H<sub>2</sub> was 3.5 L/min and 0.4 L/min, respectively. Mg acceptors were activated by annealing the Mg-doped GaN layer for 30 min at 900 °C in the presence of N<sub>2</sub> gas. The thickness of each layer, determined through cross-sectional SEM imaging, was found to be approximately 2 μm.

Physical properties and nanomechanical characteristics of both undoped GaN and Mg-doped GaN layers were analyzed by various techniques, including high-resolution X-ray diffraction (HRXRD), Raman spectroscopy, scanning electron microscopy (SEM), atomic force microscopy (AFM), and nanoindentation technique. Mg concentration was measured using a secondary ion mass spectrometry (SIMS) technique by means of EVANS EAST using an oxygen ion bombardment with an impact energy of 5.5 KeV. HRXRD was conducted on a Bruker D8 Advance diffractometer using CuKα radiation (λ = 0.154 nm). It is used to investigate the crystalline quality and structural properties of layers, where rocking

curves of symmetric and asymmetric reflections were utilized to determine the dislocation densities of edge and screw varieties. Raman spectroscopy was carried out using a micro-Raman spectrometer LABRAMHRT 4600 HR 800 with a laser excitation line of 518 nm in the frequency range of 100–1000  $\text{cm}^{-1}$ . Measurements were performed at room temperature to assess the residual stress within both samples. Zeiss Merlin Gemini II equipment high-resolution field emission scanning electron microscopy (FE-SEM) and Nanoman AFM controlled by a Nanoscope V electronics from Bruker Instruments (Bruker, Billerica, MA, USA) were used to investigate the surface morphology and roughness of the studied layers. Both samples were subjected to van der Pauw (Hall) measurement to determine their carrier concentration and resistivity. The NanoTest NT1, NanoMaterials, Ltd. instrument with a diamond Berkovich-type indenter was used to conduct nanoindentation tests. The maximum load reached was 10 mN. To obtain an average and assess the uncertainty of the measured properties, at least twenty nanoindentation tests were performed for each experimental point. The indentation cycle consisted of a loading part of 0.5 mN/s, followed by a dwell period of 30 s at the maximum load, and then an unloading phase of 0.5 mN/s until the load reached 10% of the maximum. A second hold period of 30 s was conducted to correct depth drift. In the study, the thermal drift was maintained below 0.03 nm/s for all nanoindentations. Additionally, during the first hold stage at the maximum load of 10 mN, creep behavior for both samples was examined for 30 s. To prevent possible interaction that could affect the measurement results, the indentation marks were separated by 30  $\mu\text{m}$ . SEM was utilized to investigate the indentation imprints for both undoped GaN and Mg-doped GaN layers.

### 3. Analytical Background

The technique of nanoindentation is widely used for determining the mechanical properties of nanomaterials and thin films due to its high sensitivity and precision in measuring hardness, elastic modulus, and elastic/plastic deformation characteristics. The process involves pressing a diamond indenter tip into the sample until it reaches a specified load or depth and then recording the load as a function of indenter displacement during both loading and unloading stages. The Oliver and Pharr method [16] is typically used to analyze the nanoindentation test results and determine the hardness and Young's modulus. The analysis of the test results is performed based on this method as follows:

The hardness is defined as the ratio between the maximum load  $P_{\text{max}}$  and the projected area of the indentation imprint  $A_c$ .

$$H = \frac{P_{\text{max}}}{A_c} \quad (1)$$

The ideal Berkovich indenter is only a theoretical concept that is not used in practice and results in an underestimation of the actual contact area. In reality, the imperfections in the indenter tip are considered when calculating the projected contact area using the Oliver and Pharr empirical relationship. Further details could be found in [16].

The reduced Young's modulus  $E_r$  of the thin film is expressed as follows:

$$\frac{1}{E_r} = \frac{1 - \nu^2}{E} + \frac{1 - \nu_i^2}{E_i} \quad (2)$$

where  $\nu$  and  $\nu_i$  are the Poisson coefficients of the thin film and the indenter, respectively.  $E$  and  $E_i$  are the Young's moduli of the thin film and the indenter, respectively. For the diamond indenter, Young's modulus and Poisson coefficient are  $E_i = 1141$  GPa and  $\nu_i = 0.07$ , respectively [16].

Nanoindentation is also a useful tool to study the creep behavior of a wide range of materials at the nanoscale; it can provide insights into their underlying deformation mechanism during the creep. To perform a nanoindentation creep test, the indenter is pressed into the material surface with a constant load during a period of time. The indentation depth is measured as a function of time, allowing for the determination of creep displacement

curves. Moreover, the creep rate along with the stress exponent can also be derived. It is widely accepted that uniaxial tensile tests are commonly employed to characterize the creep behavior of materials. During the steady-state creep stage, a commonly used empirical law that is applicable to a wide range of materials is as follows:

$$\dot{\epsilon} = k\sigma^n \quad (3)$$

where  $\dot{\epsilon}$  is the strain rate,  $\sigma$  is the applied stress,  $n$  is the creep stress exponent, and  $k$  is a fitting material constant. The slope of the  $\log \dot{\epsilon}$ - $\log \sigma$  curve is identified as the creep stress exponent. This parameter is very useful for giving insight into the creep mechanism of the material.

$$\dot{\epsilon} \approx \frac{1}{h} \left( \frac{dh}{dt} \right) \text{ and } \sigma \approx \frac{F}{h^2} \quad (4)$$

The computation of the displacement rate uses the derivation with respect to time of the following empirical equation given as follows [17]:

$$h(t) = h_i + a(t - t_i)^m + bt \quad (5)$$

where  $h_i$  and  $t_i$  are the initial displacement and instant of the creep;  $a$  and  $b$  are material constants of fitting.

## 4. Results and Discussion

### 4.1. Morphological, Electrical, Structural and, Vibrational Exams

Figure 1 illustrates the surface morphology of undoped and Mg-doped GaN layers. The root mean square (RMS) value of the surface roughness increases from 0.5 nm for GaN sample to 5 nm for the Mg-doped GaN sample. Previous studies reported that highly Mg-doped GaN films grown by the MOCVD process exhibit increased surface roughness and decreased free carrier concentration. This is attributed to the accumulation of Mg beyond a critical flow rate [18]. However, it is important to note that a balance between incorporating enough Mg to create p-type material and maintaining an acceptable surface morphology when manufacturing light-emitting diodes is of crucial interest [2]. The room temperature Hall measurements are used to determine the electrical properties of both samples. It was found that the hole concentration in the p-type Mg-doped GaN layer was around  $4.6 \times 10^{17} \text{ cm}^{-3}$ . The obtained result shows a slight improvement over the value reported in the literature [19]. Additionally, the electron concentration in the n-type undoped GaN layer is equal to  $4 \times 10^{17} \text{ cm}^{-3}$ . The following values of the mobility,  $280 \text{ cm}^2/\text{V.s}$ , and  $9 \text{ cm}^2/\text{V.s}$  are determined for undoped GaN and the Mg-doped GaN layer, respectively. The measured resistivity highly increases from  $0.1 \Omega \cdot \text{cm}$  for undoped GaN layer to  $2.4 \Omega \cdot \text{cm}$  for the Mg-doped GaN layer.

The threading dislocations for each sample were computed based on X-ray  $\omega$ -scans rocking curve on the (0002) and (10 $\bar{1}$ 2) diffraction peaks, which are shown in Figure 2. From these curves, the full width at half maximum of the reflections (FWHM) was assessed and used to determine the screw and edge dislocations. The threading dislocations were found equal to  $2 \times 10^8 \text{ cm}^{-2}$  and  $5 \times 10^9 \text{ cm}^{-2}$  for undoped GaN and Mg doped GaN layers, respectively. The observed increase of the threading dislocation density in Mg doped GaN layer is attributed to the presence of defects introduced during the incorporation of Mg atoms. Moreover, the use of  $\text{N}_2$  in the mixture of the carrier gas during the growth process of Mg doped GaN layer contributes to the increase of the threading dislocation density [20]. It has been earlier reported by Svensk et al. [21] that the introduction of Mg atoms contributes to the incorporation of point defects as long as  $\text{N}_2$  carrier gas is used and then the crystalline quality is spoiled. Moreover, Smorchkova et al. [22] reported that high incorporation of Mg atoms in the GaN layer leads to the formation of point defects and defect complexes, resulting in self-compensation, which is responsible for the observed low mobility and high resistivity in the p-type GaN layers, as similarly shown in this study. Kaufmann et al. [23] suggested that the nitrogen vacancy ( $V_N$ ) is a native

defect with a significant concentration in p-type GaN layers grown by MOCVD. It was found that the concentration of  $V_N$  is practically the same as that of the incorporated Mg, which is introduced through a substitutional mechanism with Ga atoms ( $Mg_{Ga}$ ). As a result, the  $Mg_{Ga}-V_N$  defect complex is formed through a self-compensation mechanism. Consequently, the observed decrease of electron mobility and the increase of resistivity of Mg doped GaN compared to undoped GaN layer corroborates the fact of introducing defects along with Mg atoms' incorporation.

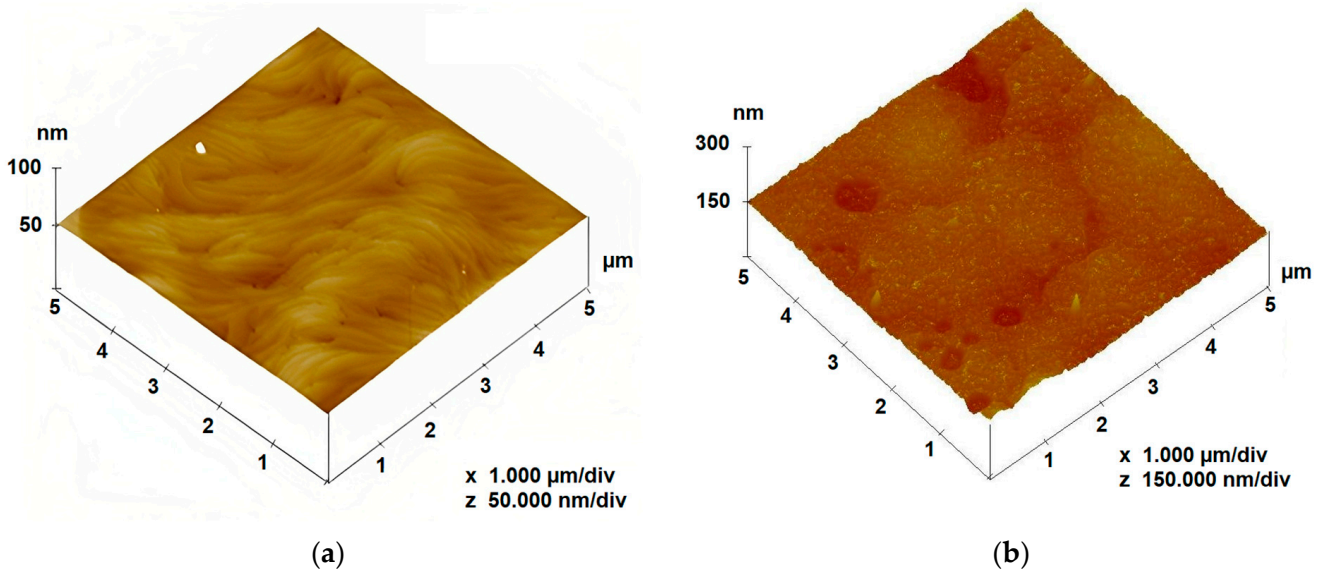


**Figure 1.** AFM images displaying the surface morphology of the grown layers: (a) undoped GaN; (b) Mg-doped GaN layer.

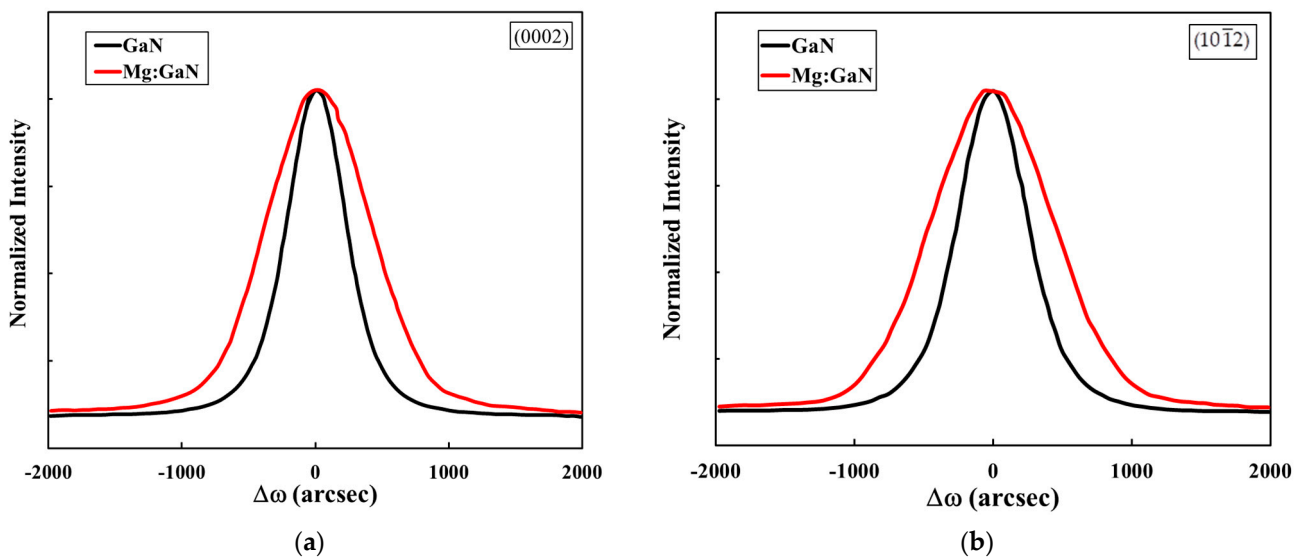


**Figure 2.** X-ray  $\omega$  scans (rocking curve) of: (a) (0002) reflection; (b)  $(10\bar{1}2)$  reflection of undoped GaN and Mg-doped GaN layers.

Figure 3 shows the SIMS depth profiles for the Mg-doped GaN layer. It reveals that the concentration of Mg atoms is about  $2 \times 10^{19}$  atom/cm<sup>3</sup>. In addition, the Mg concentration was found homogeneously distributed across the thickness of the sample.

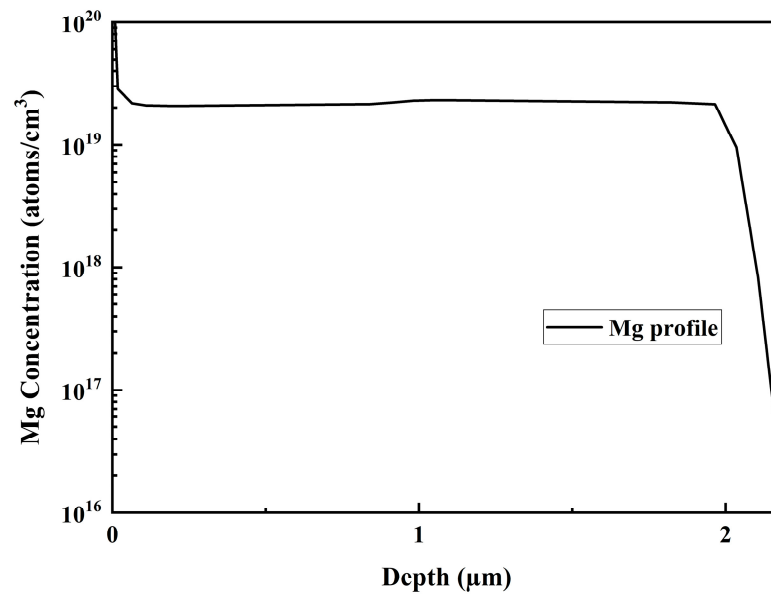


Figure 3. SIMS depth profiles of Mg atoms for the Mg-doped GaN layer.

Figure 4 exhibits the Raman spectra of undoped GaN and Mg-doped GaN layers. The analysis of these spectra allows for the determination the stress states in both samples using the intense  $E_2$  (high) phonon frequency mode. This enables a direct comparison of the stress states relative to a reference peak [20]. The strain-free frequency of the  $E_2$  (high) phonon mode for the GaN bulk layer is located at  $566.34 \text{ cm}^{-1}$  [21] and it is represented by the dashed line. Both layers are under compressive stresses as they are located on the right side of the bulk GaN position. The spectrum of the Mg-doped GaN layer showed weakening and broadening of the  $E_2$  (high) peak at  $568.4 \text{ cm}^{-1}$ , indicating lower crystalline quality compared to the  $E_2$  (high) peak at  $566.8 \text{ cm}^{-1}$  for the undoped GaN layer. Moreover, the introduction of Mg atoms induced higher compressive stress in the Mg-doped GaN layer compared to undoped GaN, leading to a shift of the  $E_2$  (high) peak towards higher wave numbers. To quantitatively assess the residual stresses inherent in both layers, the  $E_2$  (high) peaks are used to calculate these stresses using the method as reported in [22]. It was found that  $\sigma_{\text{undoped GaN}} = -0.10 \text{ GPa}$  and  $\sigma_{\text{Mg doped GaN}} = -0.47 \text{ GPa}$ . The minus sign (–) indicates that the residual stresses are of a compressive nature.

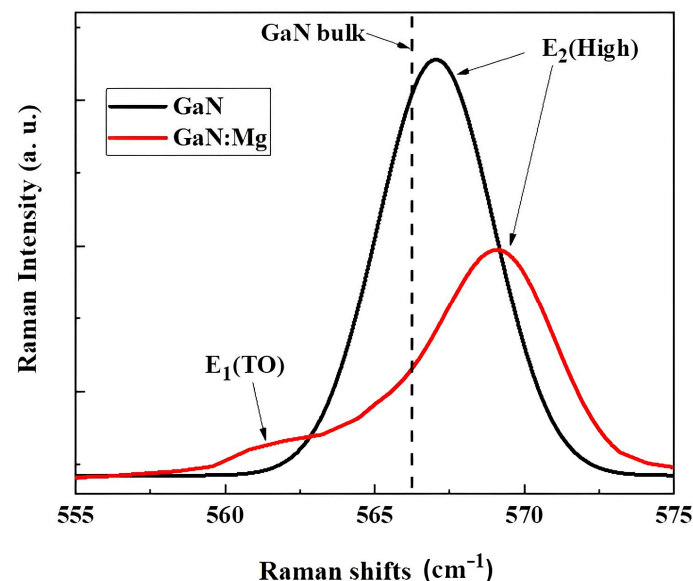
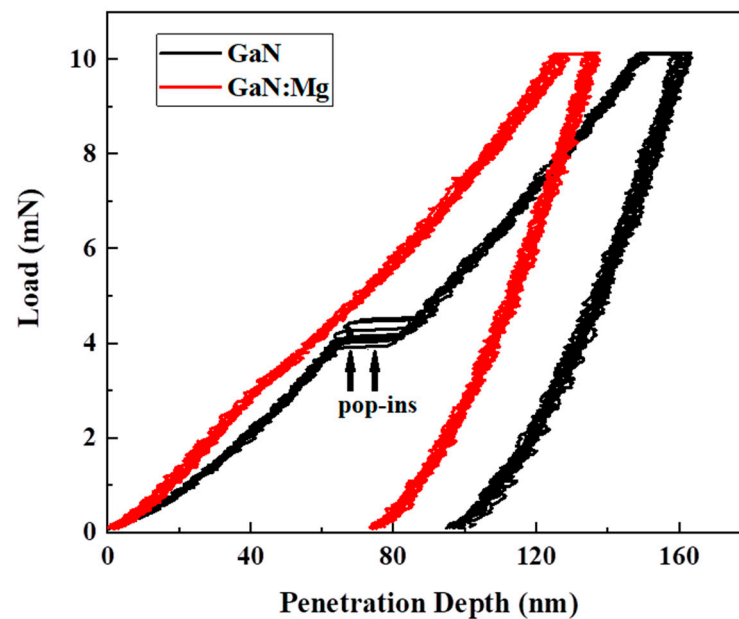


Figure 4. Raman spectra of undoped and Mg-doped GaN layers measured at room temperature.

This behavior was explained by the difference in size between the dopant atom radius ( $r_{\text{Mg}} = 0.136 \text{ nm}$ ) and the replaced host atom radius ( $r_{\text{Ga}} = 0.126 \text{ nm}$ ). Additionally, it was observed that the incorporated Mg atoms contributed to disclose the  $E_1$  (TO) phonon mode at  $561 \text{ cm}^{-1}$ , indicating disorder in the Mg-doped GaN layer accredited to the presence of high concentrations of defects [22], when compared to the undoped GaN layer. Subsequently, the analysis of Raman spectra provides valuable insight into the effects of Mg doping on the lattice vibrational properties of GaN layers, including the emergence of new phonon modes.

#### 4.2. Nanoindentation Tests Analysis

Figure 5 shows the load–unload nanoindentation curves obtained for both undoped and Mg-doped GaN layers carried out at the maximal load  $P_{\text{max}} = 10 \text{ mN}$ . It clearly reveals the different features between both grown layers. The load–unload curve for the undoped GaN layer depicts the first pop-in events (sudden burst during the loading curve) corresponding to the critical load  $P_c$  around 4 mN and the length of the plateau is about 20 nm, for which the incipient plasticity of the GaN layer was initiated under the effect of yielding shear stress  $\tau_{\text{max}}$ . The dissipated energy for the formation of the pop-ins is approximately  $8 \times 10^{-12} \text{ J}$ . However, for the Mg-doped GaN layer, the elastic–plastic transition occurred without the appearance of the pop-in events.



**Figure 5.** Load–unload nanoindentation curves recorded for undoped GaN and Mg-doped GaN layers. The indentation curve for the undoped GaN layer clearly discloses pop-in events that indicate the onset of the elastic–plastic transition. For the Mg-doped GaN curve, the elastic–plastic transition occurred without the appearance of pop-in events.

The yielding shear stress  $\tau_{\text{max}}$ , for which the plastic deformation initiated locally underneath the indenter tip, is calculated using Johnson’s relationship [23] and is expressed as follows:

$$\tau_{\text{max}} = 0.31 \left( \frac{6P_c E^2}{\pi^3 R^2} \right)^{1/3} \quad (6)$$

where  $P_c$ ,  $E$ , and  $R$  are the critical load, the Young’s modulus and the indenter tip radius, respectively. The critical load corresponds to the load that initiates the elastic–plastic transition. For the load–unload curves that present pop-in events, the critical load is directly observed. However, for the load–unload curves for which no pop-in events are revealed, the load for the transition between the elastic and plastic is obtained using the divergence point between loading curve and the curve representing the Hertz equation

(Hertz contact theory) [23]. Moreover, it is noticed that the maximal depth penetration for the Mg-doped GaN layer is lower than that for the undoped GaN layer. This latter assumes that the resistance to the penetration of the indenter tip to further plastically deform the Mg-doped GaN layer is higher for the same applied load than that for the undoped GaN layer.

Thus, it is expected that the hardness of the Mg-doped GaN layer is higher than that for the GaN layer. In addition, it is worth noting that at the maximal load  $P_{\max}$  and for holding time equal to 30 s, the depth penetration obtained for the Mg-doped GaN layer is lower than that revealed for the GaN layer. In this stage, the evolution of the plastic deformation for a constant load and during a period of time is attributed to the creep phenomenon, which is thoroughly investigated in the next section.

In order to corroborate these qualitative observations, mechanical properties were determined for both samples; namely the hardness  $H$ , the Young's modulus  $E$ , the maximal shear stress  $\tau_{\max}$ , the plastic work  $Wp$ , and the  $H/E$  ratio. Table 1 lists these mechanical properties along with findings documented in literature for comparison purposes.

**Table 1.** Mechanical properties of undoped and Mg-doped GaN layers obtained in this study compared to those reported in the literature.

Sample	Hardness $H$ (GPa)	Young's Modulus $E$ (GPa)	Plastic Work ( $\times 10^{-12}$ J) $Wp$	Maximal Shear Stress $\tau_{\max}$ (GPa)	$H/E$
Undoped GaN #	$17.7 \pm 0.9$	$340.3 \pm 10.7$	$472 \pm 28$	$23.1 \pm 0.7$	0.052
[24]	20.0	323.8	-	$18.9 \pm 1.3$	-
[10]	$19 \pm 1$	$286 \pm 25$	0.7	6.3	-
Mg-doped GaN #	$21.3 \pm 1.4$	$410.2 \pm 11.3$	$437 \pm 21$	$20.7 \pm 0.5$	0.052
[10]	$22.3 \pm 1.2$	$333.2 \pm 8.2$	4.1	$7.5 \pm 0.4$	-

# This study.

The analysis of the results presented in this table shows that the hardness and Young's modulus of the Mg-doped GaN layer are higher than those measured for the undoped GaN layer. In other words, Mg-doped GaN thin film is harder and stiffer due to the strengthening effect of the Mg atoms in the crystal lattice, but it may also be less ductile due to the pinning of dislocations by the Mg atoms that can act to inhibit dislocations' motion [25]. As a result, the plastic work of the Mg-doped GaN layer is lower than that of the undoped GaN layer. Additionally, it is important to note that the maximal shear stress calculated for the undoped GaN layer is slightly higher than that obtained for the Mg-doped GaN layer. The maximal shear stress is the stress at which the transition from the elastic to the plastic regime is initiated. The observed difference in the maximal shear stress is attributed to the appearance of pop-in events in the undoped GaN layer, which are absent in the Mg-doped GaN layer due to the dissimilar defect densities; and thus due to the different dislocation mechanisms that are undergone in each sample during nanoindentation tests. Moreover, it is worth noting that the values of hardness and Young's modulus in Table 1 show some degree of scattering compared to the literature. Several examples are documented in reference [9]. This scattering can be attributed to various factors, such as different growth conditions and processes of GaN [26], the applied maximal forces [27], nanoindentation instrumentation techniques (e.g., continuous contact stiffness measurements (CSM)) [28], and different indenter types [29], etc. However, our findings are included in the range of the mechanical properties documented in the literature. Furthermore, it is worth mentioning that there is limited literature available regarding the mechanical properties of Mg-doped GaN layers [10].

Pop-in events are sudden and large plastic deformations can occur during nanoindentation, usually for materials featured by low dislocation density. These events are often associated with the homogeneous nucleation and emission of dislocations is activated [30]. In the case of undoped GaN layers, the presence of low dislocation density as low as

$2 \times 10^8 \text{ cm}^{-2}$  can lead to the formation of pop-in events during nanoindentation and can lead to a higher degree of plastic deformation. These dislocations are nucleated and propagated through the material in response to the shear stress applied by the indenter, leading to the observed pop-in events. However, in Mg-doped GaN layers, the absence of these pop-ins suggests a different mechanism of plastic deformation as what could be associated to the undoped GaN layer. The pinning of dislocations by Mg atoms can inhibit the homogeneous nucleation of dislocations, preventing the formation of pop-in events. Instead, plastic deformation in Mg-doped GaN may occur through a collective activation of mobile dislocations due to its higher dislocation density compared to that of the undoped GaN layer. In this mechanism, dislocations that are already present in the material are activated by the applied stress and move collectively to accommodate the accumulated strains. To support these findings regarding the observed pop-in events, it is worth noting that previous studies demonstrated a significant influence of the pre-existing density of dislocations on the occurrence of pop-in events [9,31]. Lorenz et al. [32] indicated that pop-in events will not occur when the dislocation density is greater than  $10^9 \text{ cm}^{-2}$  for a high indenter tip radius. Here, it is worth noting that the radius  $R$  of the Berkovich indenter tip used in this study was evaluated to be  $500 \pm 10 \text{ nm}$  using the Hertz contact theory.

The calculated  $H/E$  ratio is found similar for both thin films. This ratio is a measure of a material's resistance to plastic deformation, with higher values indicating greater resistance. Furthermore, this ratio can be also used to compute the fracture toughness of materials  $K_{IC}$ , as it is inversely proportional to fracture toughness [33]. The fact that the  $H/E$  ratio is the same for both types of thin films indicates that they likely have similar resistance to crack propagation despite the observed differences in their mechanical strength and stiffness. Nevertheless, it is important to note that in the current study, our aim is not measuring the fracture toughness  $K_{IC}$  of both samples, which would require indentations with an appropriate load to induce cracks.

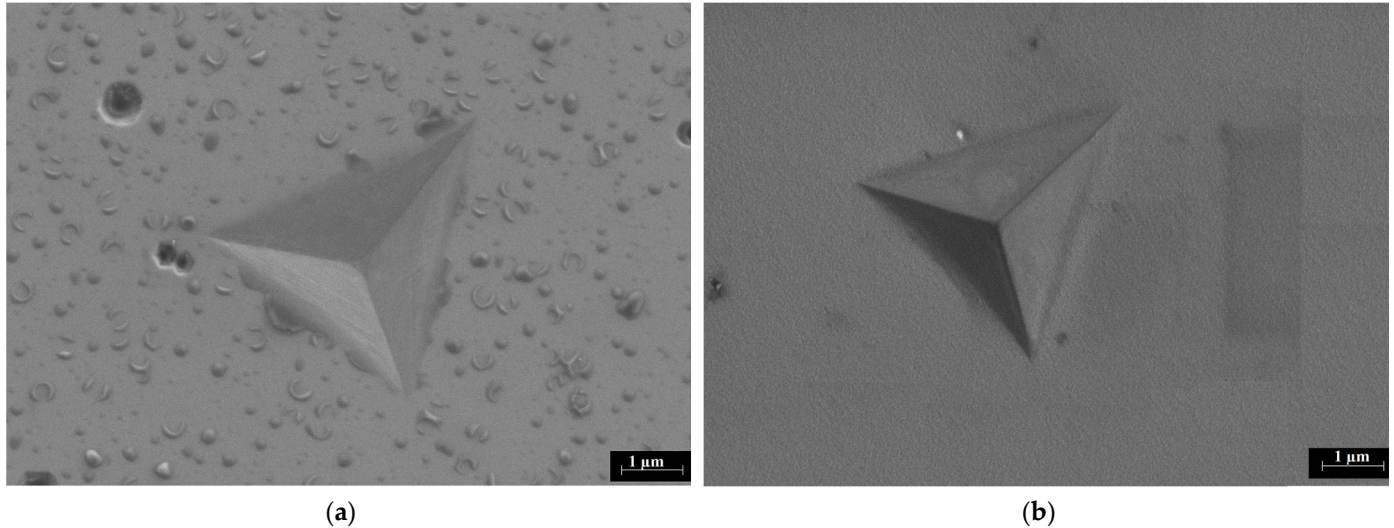
In summary, the presence or absence of pop-in events during the nanoindentation of undoped and Mg-doped GaN layers is indicative of different mechanisms of plastic deformation, which can be attributed to the presence or absence of dislocation pinning by magnesium atoms. The mechanism of plastic deformation can affect the maximal shear stress of the material, with undoped GaN having a higher maximal shear stress due to its ability to deform plastically through homogeneous dislocation nucleation. Though, no effect was observed on the  $H/E$  ratio of both types of thin films. Thus, the findings could have implications for the design and development of GaN thin films for various applications, including microelectromechanical devices, sensors, and optoelectronics.

Figure 6 shows imprints of the Berkovich indenter tip on both the undoped and Mg-doped GaN layers, which were subjected to a maximal loading charge of 500 mN. No cracks were detected during this high loading, which was likely due to the good fracture toughness of both samples. Such behavior could be interpreted by the lower  $H/E$  ratio calculated for both samples. The undoped GaN shows a slightly ductile behavior, where it is possible to undergo more plastic strains by applying local severe shear stresses, when compared to the Mg-doped GaN layer.

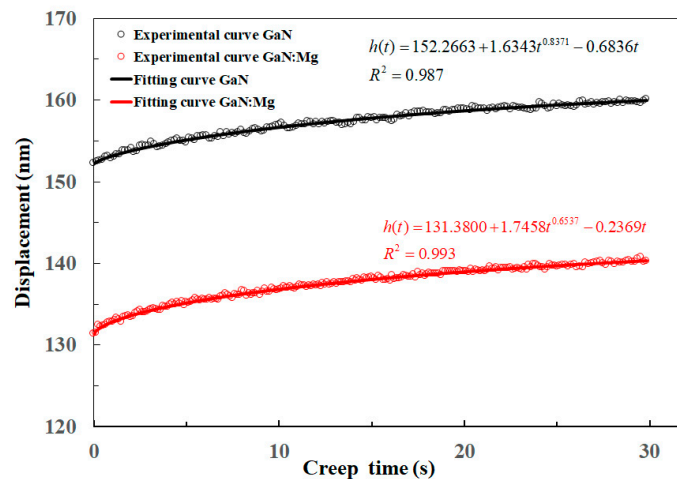
#### 4.3. Creep Behavior Analysis

Figure 7 exhibits a comparison of the creep displacement versus time during a 30 s dwell period for both undoped GaN and Mg-doped GaN layers. For both curves, the fitting curve shows a very good adjustment for the experimental points, with correlation coefficients above 0.98. The results indicate that both types of layers undergo an initial rapid increase in creep displacement, followed by a subsequent reduction in the rate of creep displacement. Notably, the displacement curve for the undoped GaN layer is positioned higher than that for the Mg-doped GaN layer, indicating that at a constant load of 10 mN, undoped GaN is more susceptible to plastic deformation during creep than Mg-doped GaN. The maximum indentation depth observed during the 30 s dwell period is higher for the undoped GaN than for the Mg-doped GaN. This variation is likely due to different

dislocation mechanisms that are undergone at the initiation of the creep stage and to the dislocation density formed beneath the indenter in both types of GaN layers, which subsequently affect the creep behavior.



**Figure 6.** SEM images of imprinted zones using a 500 mN loading charge with Berkovich indenter showing no microcracks: (a) undoped GaN layer; (b) Mg-doped GaN layer.

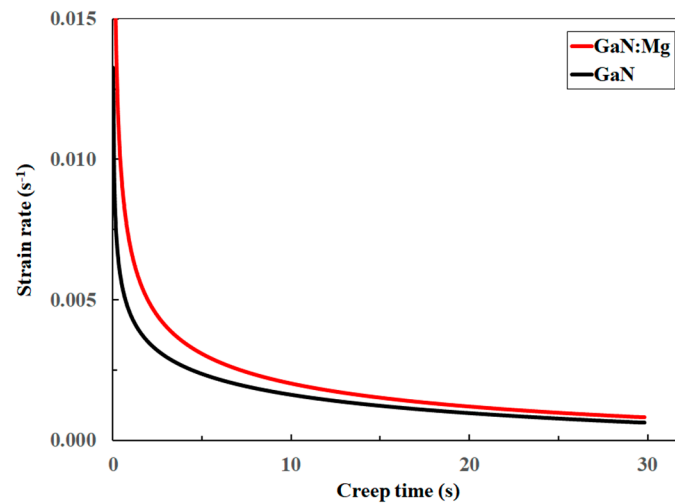


**Figure 7.** Creep displacement vs. the creep time for both undoped GaN and Mg-doped GaN (GaN:Mg) layers using a maximum indentation force of 10 mN.

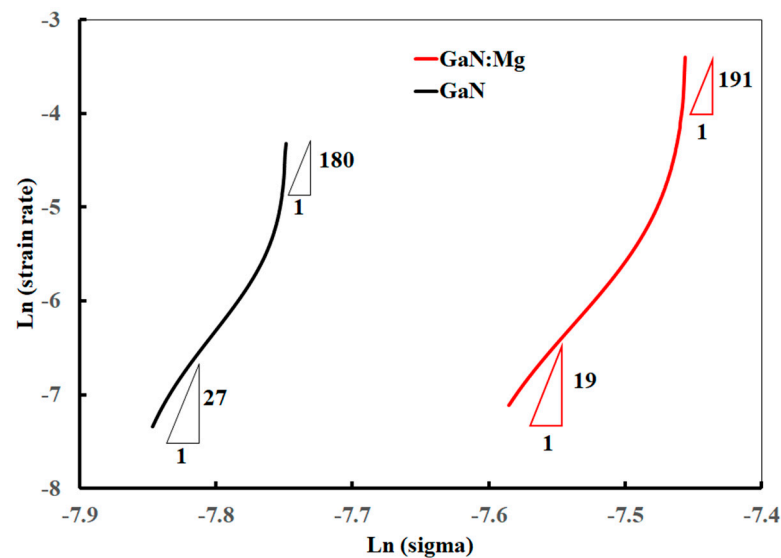
Furthermore, we plotted in Figure 8 the creep strain rate  $\dot{\epsilon}$  as a function of creep time (during the dwell time) for both types of samples and calculated it using Equation (4). During the initial stage of the creep process, the strain rate was very high, then it abruptly decreased to reach a strain rate of around  $2 \times 10^{-3} \text{ s}^{-1}$  in less than 10 s. This initial stage of creep is called transient creep. Thereafter, the strain rate is gradually decreased to converge progressively towards a steady-state creep regime, which is called secondary creep. In the steady-state regime, the creep strain rate is so low that its effect on the modulus result is negligible.

Figure 9 shows the evolution of  $\ln \dot{\epsilon}$  vs.  $\ln \sigma$  to derive the creep stress exponent during the steady-state regime, revealing the real nanoindentation creep properties of both samples. The stress exponent  $n = (\partial \ln \dot{\epsilon} / \partial \ln \sigma)$  is instantaneous property, which varies along with the applied stress underneath the indenter tip. To gain a deeper understanding of the observed phenomenon and to question the time-dependent plastic deformation mechanism developed during the creep process, it is crucial to probe the creep stress exponent in

the steady-state creep regime. It is evident that the creep stress exponent is higher for the undoped GaN layer. Furthermore, it is observed that higher hardness and Young’s modulus are associated with a lower stress exponent. Since the maximum applied load is similar for both types of samples, the correlation between hardness and the related stress exponent is likely due to the severity encountered to further plastically deform the volume localized underneath the indenter. It was previously established that the stress exponent is proportional to the sheared volume [34]. As the indent size increases (i.e., for lower hardness materials), the plastically deformed volume also increases, leading to a decrease in the stress exponent. Additionally, the creep stress exponent is typically considered as a useful indicator for identifying the predominant creep mechanism. For instance, for  $n = 1$ , the observed dominant mechanism is the diffusion creep mechanism involving vacancy flow through the lattice, known as the Nabarro–Herring creep. However, for a creep stress exponent greater than 3, the creep mechanism is governed by dislocation glides and climbs (power-law creep equation) [35].



**Figure 8.** Creep strain rate as a function of the creep time for undoped GaN and Mg-doped GaN (GaN:Mg) layers using a maximum indentation force of 10 mN.



**Figure 9.** Logarithmic creep strain rate versus logarithmic stress curves for undoped GaN and Mg-doped GaN (GaN:Mg) samples under a load of 10 mN during the creep time of 30 s.

The tested samples exhibited a high creep stress exponent. In the Mg-doped GaN layer, the stress exponent was found to be 19, compared to 27 for the undoped GaN layer

(i.e., greater than three), indicating that the creep behavior observed in both samples is governed by the mechanism of dislocation glides and climbs.

In addition, it should be noted that the nanoindentation creep is sensitive to experimental conditions, including the initial loading and unloading phases of the cycle. During the nanoindentation test, the hardness and Young's modulus were measured and found to increase in the case of Mg-doped GaN compared with the undoped GaN layer. However, the steady-state regime of the nanoindentation creep is influenced by significant creep effects, which can affect the measured Young's modulus. The Oliver–Pharr method [16] was employed to measure the Young's modulus, which assumes a purely elastic contact during the unloading stage. Nevertheless, this assumption is not always valid due to thermal drift effects, and creep effects can cause an overestimation of the contact stiffness, thereby influencing the measured Young's modulus. To obtain accurate measurements of the hardness and Young's modulus, a holding time of 30 s was considered sufficient to mitigate any potential creep effects on the measured values, as suggested by Chudoba et al. [36]. The drift rate during this time was estimated to be 0.01 nm/s, which is typically low.

## 5. Conclusions

This paper investigates the physical and nanomechanical properties of undoped and Mg-doped GaN layers deposited on sapphire substrates using the MOCVD technique. Various probing techniques were employed to analyze the effect of Mg incorporation compared to the undoped GaN layer, on the morphological, electrical, structural, lattice vibrational properties, nanomechanical properties, and creep behavior. The incorporation of Mg resulted in a transition from n-type to p-type conductivity, which led to an increase in defects and the disappearance of pop-ins that were observed in the loading–unloading nanoindentation curve of the undoped GaN layer. Furthermore, a rise in the nanomechanical properties of the Mg-doped GaN layer was revealed, as seen in the increased hardness and Young's modulus. This is attributed to the different dislocation mechanisms that occurred in both GaN samples during the nanoindentation tests. However, the H/E ratio was found to be alike for both layers, assuming a likely similar fracture resistance feature. The introduction of controlled defects in Mg-doped GaN layers can offer a favorable balance between improved physical properties and high-strength semiconductor materials. This suggests the potential application of Mg-doped GaN layers in optoelectronic devices.

From a mechanical standpoint, the hardening effect was attributed to an increase in the pre-existing dislocation density and the introduction of point defects underneath the indenter tip during the incorporation of Mg doping into the GaN layers. This led to a decrease in the creep stress exponent and creep depth, which are related to the inherent creep mechanism governed by dislocation glides and climbs. Therefore, this study emphasizes the importance of understanding the correlation between the physical properties and mechanical characteristics of undoped and Mg-doped GaN thin films, which may have significant implications for a wide range of technological applications.

**Author Contributions:** Conceptualization, A.K. and Z.B.; methodology, A.K. and Z.B.; investigation, A.K. and Z.B.; validation, A.K. and Z.B.; formal analysis, A.K. and Z.B.; data curation, A.K. and Z.B.; writing—original draft preparation, A.K.; writing—review and editing, A.K. and Z.B. All authors have read and agreed to the published version of the manuscript.

**Funding:** This research received no external funding.

**Institutional Review Board Statement:** Not applicable.

**Informed Consent Statement:** Not applicable.

**Data Availability Statement:** Not applicable.

**Acknowledgments:** Zohra Benzarti gratefully acknowledge her support by FEDER funds through the program COMPETE and by the project AM4SP (code POCI-01-0247-FEDER-070521), co-funded by FCT, Portuguese Foundation for Science and Technology and POCI 2020 through the program

Portugal 2020. The authors thank the support to this investigation by M. Evaristo and by A. Cavaleiro from CEMMPRE @ University of Coimbra in Portugal.

**Conflicts of Interest:** The authors declare no conflict of interest.

## References

1. Yoshida, S. Growth of Cubic III-Nitride Semiconductors for Electronics and Optoelectronics Application. *Phys. E Low-Dimens. Syst. Nanostructures* **2000**, *7*, 907–914. [[CrossRef](#)]
2. Benzarti, Z.; Sekrafi, T.; Bougrioua, Z.; Khalfallah, A.; El Jani, B. Effect of SiN Treatment on Optical Properties of In<sub>x</sub>Ga<sub>1-x</sub>N/GaN MQW Blue LEDs. *J. Electron. Mater.* **2017**, *46*, 4312–4320. [[CrossRef](#)]
3. Zheng, Y.; Sun, C.; Xiong, B.; Wang, L.; Hao, Z.; Wang, J.; Han, Y.; Li, H.; Yu, J.; Luo, Y. Integrated Gallium Nitride Nonlinear Photonics. *Laser Photonics Rev.* **2022**, *16*, 2100071. [[CrossRef](#)]
4. Benzarti, Z.; Halidou, I.; Bougrioua, Z.; Boufaden, T.; El Jani, B. Magnesium Diffusion Profile in GaN Grown by MOVPE. *J. Cryst. Growth* **2008**, *310*, 3274–3277. [[CrossRef](#)]
5. Pengelly, R.S.; Wood, S.M.; Milligan, J.W.; Sheppard, S.T.; Pribble, W.L. A Review of GaN on SiC High Electron-Mobility Power Transistors and MMICs. *IEEE Trans. Microw. Theory Tech.* **2012**, *60*, 1764–1783. [[CrossRef](#)]
6. Abdul Amir, H.A.A.; Fakhri, M.A.; Abdulkhaleq Alwahib, A. Review of GaN Optical Device Characteristics, Applications, and Optical Analysis Technology. *Mater. Today Proc.* **2021**, *42*, 2815–2821. [[CrossRef](#)]
7. Azimah, E.; Zainal, N.; Hassan, Z.; Shuhaimi, A.; Bahrin, A. Electrical and Optical Characterization of Mg Doping in GaN. *Adv. Mater. Res.* **2013**, *620*, 453–457. [[CrossRef](#)]
8. Sun, L.; Weng, G.E.; Liang, M.M.; Ying, L.Y.; Lv, X.Q.; Zhang, J.Y.; Zhang, B.P. Influence of P-GaN Annealing on the Optical and Electrical Properties of InGa<sub>N</sub>/Ga<sub>N</sub> MQW LEDs. *Phys. E Low-Dimens. Syst. Nanostructures* **2014**, *60*, 166–169. [[CrossRef](#)]
9. Boughrara, N.; Benzarti, Z.; Khalfallah, A.; Evaristo, M.; Cavaleiro, A. Comparative Study on the Nanomechanical Behavior and Physical Properties Influenced by the Epitaxial Growth Mechanisms of GaN Thin Films. *Appl. Surf. Sci.* **2022**, *579*, 152188. [[CrossRef](#)]
10. Jian, S.R.; Ke, W.C.; Juang, J.Y. Mechanical Characteristics of Mg-Doped GaN Thin Films by Nanoindentation. *Nanosci. Nanotechnol. Lett.* **2012**, *4*, 598–603. [[CrossRef](#)]
11. Li-Jun, D.; Yuzhen, L.; Dapeng, C.; Wang, X. Green-Blue Luminescence from the Silicon-Rich Silicon Nitride Thin Films. *Chin. J. Lumin.* **2005**, *26*, 380–384.
12. Prado, E.O.; Bolsi, P.C.; Sartori, H.C.; Pinheiro, J.R. An Overview about Si, Superjunction, SiC and GaN Power MOSFET Technologies in Power Electronics Applications. *Energies* **2022**, *15*, 5244. [[CrossRef](#)]
13. Wang, S.; Hung, N.T.; Tian, H.; Islam, M.S.; Saito, R. Switching Behavior of a Heterostructure Based on Periodically Doped Graphene Nanoribbon. *Phys. Rev. Appl.* **2021**, *16*, 024030. [[CrossRef](#)]
14. Lin, J.T.; Wang, P.; Shuvra, P.; McNamara, S.; McCurdy, M.; Davidon, J.; Walsh, K.; Alles, M.; Alphenaar, B. Impact of X-Ray Radiation on GaN/AlN MEMS Structure and GaN HEMT Gauge Factor Response. In Proceedings of the IEEE 33rd International Conference on Micro Electro Mechanical Systems (MEMS), Vancouver, BC, Canada, 18–22 January 2020; pp. 968–971. [[CrossRef](#)]
15. Boughrara, N.; Benzarti, Z.; Khalfallah, A.; Oliveira, J.C.; Evaristo, M.; Cavaleiro, A. Thickness-Dependent Physical and Nanomechanical Properties of Al<sub>x</sub>Ga<sub>1-x</sub>N Thin Films. *Mater. Sci. Semicond. Process.* **2022**, *151*, 107023. [[CrossRef](#)]
16. Oliver, W.C.; Pharr, G.M. An Improved Technique for Determining Hardness and Elastic Modulus Using Load and Displacement Sensing Indentation Experiments. *J. Mater. Res.* **1992**, *7*, 1564–1583. [[CrossRef](#)]
17. Li, H.; Ngan, A.H.W. Size Effects of Nanoindentation Creep. *J. Mater. Res.* **2004**, *19*, 513–522. [[CrossRef](#)]
18. Bethoux, J.M.; Vennéguès, P.; Natali, F.; Felten, E.; Tottereau, O.; Nataf, G.; De Mierry, P.; Semond, F. Growth of High Quality Crack-Free AlGa<sub>N</sub> Films on GaN Templates Using Plastic Relaxation through Buried Cracks. *J. Appl. Phys.* **2003**, *94*, 6499–6507. [[CrossRef](#)]
19. Liu, S.T.; Yang, J.; Zhao, D.G.; Jiang, D.S.; Liang, F.; Chen, P.; Zhu, J.J.; Liu, Z.S.; Liu, W.; Xing, Y.; et al. Influence of Carrier Gas H<sub>2</sub> Flow Rate on Quality of P-Type GaN Epilayer Grown and Annealed at Lower Temperatures. *Chin. Phys. B* **2018**, *27*, 127803. [[CrossRef](#)]
20. Kozawa, T.; Kachi, T.; Kano, H.; Nagase, H.; Koide, N.; Manabe, K. Thermal Stress in GaN Epitaxial Layers Grown on Sapphire Substrates. *J. Appl. Phys.* **1995**, *77*, 4389–4392. [[CrossRef](#)]
21. Cho, Y.S.; Hardtdegen, H.; Kaluza, N.; Thillosen, N.; Steins, R.; Sofer, Z.; Lüth, H. Effect of Carrier Gas on GaN Epilayer Characteristics. *Phys. Status Solidi* **2006**, *3*, 1408–1411. [[CrossRef](#)]
22. Kunert, H.W.; Brink, D.J.; Auret, F.D.; Maremane, M.; Prinsloo, L.C.; Barnas, J.; Beaumont, B.; Gibart, P. Photoluminescence and Raman Spectroscopy of Mg-Doped GaN; As Grown, Hydrogen Implanted and Annealed. *Mater. Sci. Eng. B Solid State Mater. Adv. Technol.* **2003**, *102*, 293–297. [[CrossRef](#)]
23. Johnson, K.L. *Contact Mechanics*; Cambridge University Press: Cambridge, UK, 1985; ISBN 9780521255769.
24. Fujikane, M.; Inoue, A.; Yokogawa, T.; Nagao, S.; Nowak, R. Mechanical Properties Characterization of c-Plane (0001) and m-Plane (10-10) GaN by Nanoindentation Examination. *Phys. Status Solidi* **2010**, *7*, 1798–1800. [[CrossRef](#)]
25. Shuldiner, A.V.; Zakrevskii, V.A. The Mechanism of Interaction of Dislocations with Point Defects in Ionic Crystals. *J. Phys. Condens. Matter* **2002**, *14*, 9555–9562. [[CrossRef](#)]

26. García Hernández, S.A.; Compeán García, V.D.; López Luna, E.; Vidal, M.A. Elastic Modulus and Hardness of Cubic GaN Grown by Molecular Beam Epitaxy Obtained by Nanoindentation. *Thin Solid Films* **2020**, *699*, 137915. [[CrossRef](#)]
27. Jian, S.R.; Fang, T.H.; Chuu, D.S. Analysis of Physical Properties of III-Nitride Thin Films by Nanoindentation. *J. Electron. Mater.* **2003**, *32*, 496–500. [[CrossRef](#)]
28. Yang, P.F.; Huang, C.C.; Chen, D.L.; Lin, T.C.; Tsai, Y.H.; Jian, S.R. Nanomechanical Properties and Fracture Behaviors of GaN and Al<sub>0.08</sub>Ga<sub>0.92</sub>N Thin Films Deposited on c-Plane Sapphire by MOCVD. In Proceedings of the 2016 11th International Microsystems, Packaging, Assembly and Circuits Technology Conference (IMPACT), Taipei, Taiwan, 26–28 October 2016; Technical Paper. pp. 349–352. [[CrossRef](#)]
29. Fujikane, M.; Leszczyński, M.; Nagao, S.; Nakayama, T.; Yamanaka, S.; Niihara, K.; Nowak, R. Elastic-Plastic Transition during Nanoindentation in Bulk GaN Crystal. *J. Alloys Compd.* **2008**, *450*, 405–411. [[CrossRef](#)]
30. Benzarti, Z.; Sekrafi, T.; Khalfallah, A.; Bougrioua, Z.; Vignaud, D.; Evaristo, M.; Cavaleiro, A. Growth Temperature Effect on Physical and Mechanical Properties of Nitrogen Rich InN Epilayers. *J. Alloys Compd.* **2021**, *885*, 160951. [[CrossRef](#)]
31. Lodes, M.A.; Hartmaier, A.; Göken, M.; Durst, K. Influence of Dislocation Density on the Pop-in Behavior and Indentation Size Effect in CaF<sub>2</sub> Single Crystals: Experiments and Molecular Dynamics Simulations. *Acta Mater.* **2011**, *59*, 4264–4273. [[CrossRef](#)]
32. Lorenz, D.; Zeckzer, A.; Hilpert, U.; Grau, P.; Johansen, H.; Leipner, H.S. Pop-in Effect as Homogeneous Nucleation of Dislocations during Nanoindentation. *Phys. Rev. B Condens. Matter Mater. Phys.* **2003**, *67*, 172101. [[CrossRef](#)]
33. Lawn, B.R.; Evans, A.G.; Marshall, D.B. Elastic/Plastic Indentation Damage in Ceramics: The Median/Radial Crack System. *J. Am. Ceram. Soc.* **1980**, *63*, 574–581. [[CrossRef](#)]
34. Argon, A. Plastic Deformation in Metallic Glasses. *Acta Metall.* **1979**, *27*, 47–58. [[CrossRef](#)]
35. Choi, I.C.; Yoo, B.G.; Kim, Y.J.; Jang, J. II Indentation Creep Revisited. *J. Mater. Res.* **2012**, *27*, 3–11. [[CrossRef](#)]
36. Chudoba, T.; Richter, F. Investigation of Creep Behaviour under Load during Indentation Experiments and Its Influence on Hardness and Modulus Results. *Surf. Coat. Technol.* **2001**, *148*, 191–198. [[CrossRef](#)]

**Disclaimer/Publisher's Note:** The statements, opinions and data contained in all publications are solely those of the individual author(s) and contributor(s) and not of MDPI and/or the editor(s). MDPI and/or the editor(s) disclaim responsibility for any injury to people or property resulting from any ideas, methods, instructions or products referred to in the content.